Site Characterization with 3-D Full Seismic Waveform Tomography

Khiem T. Tran, Ph.D.[1]; and Trung Dung Nguyen[2]

[1]Assistant Professor, Dept. of Civil and Environmental Engineering, Clarkson Univ., P.O. Box 5710, Potsdam, NY 13699-5710. E-mail: ktran@clarkson.edu
[2]Ph.D. Student, Dept. of Civil and Environmental Engineering, Clarkson Univ., P.O. Box 5710, Potsdam, NY 13699-5710. E-mail: nguyent@clarkson.edu

Abstract

A new three-dimensional full waveform inversion (3D FWI) method is presented for geotechnical site characterization. The method is based on a solution of 3D elastic wave equations for forward modeling to simulate wave propagation, and a cross-adjoint gradient approach for model updating to extract material property. The staggered-grid finite-difference technique is used to solve the wave equations, together with implementation of the perfectly matched layer condition for boundary truncation. The gradient is calculated from the forward and backward wavefields. Reversed-in-time displacement residuals are induced as multiple sources at all receiver locations for simulation of the backward wavefield. Seismic wavefields are acquired from geophysical testing using sensors and sources located in uniform 2D grids on the ground surface, and then inverted for extraction of 3D subsurface wave velocity structures. The capability of the presented FWI method is tested on both synthetic and field experimental datasets. The inversion results from synthetic data show the 3D FWI ability in characterizing laterally variable low- and high-velocity layers. Field experimental data were collected using 96 receivers and a propelled energy generator (PEG) to generate seismic wave energy. The field data result shows that the waveform analysis was able to delineate variable subsurface soil layers. The seismic inversion results are generally consistent with invasive standard penetration test (SPT) N-values, including identification of a low-velocity zone.

INTRODUCTION

Site characterization is important for successful design of substructures, as unanticipated site conditions such as highly variable soil/rock layers with embedded low-velocity anomalies (soft soils) cause significant problems during and after construction of foundations. Surface-based seismic methods are often used for geotechnical site characterization to assess spatial variation and material properties. They include surface wave, refraction tomography, and full waveform tomography methods. The surface wave method such as multichannel analysis of surface waves (MASW) uses dispersive characteristic of Rayleigh waves to determine 1-D S-wave velocity (V_S) profiles. This method tends to average V_S values over considerable volumes of material, and it is not very sensitive to thin embedded low-velocity layers. Refraction tomography uses the first-arrival times to determine P-wave velocity (V_P) profiles. As the first-arrival signals tend to propagate through high-velocity layers, embedded low-velocity layers are not well characterized.

As reviewed by Vireux and Operto (2009), by extracting information contained in the complete waveforms, the full waveform inversion (FWI) approach offers the potential to produce higher resolution models of the subsurface structures than approaches that consider only the dispersive characteristic of Rayleigh waves or first-arrival times of body waves. The FWI

approach could be used to identify and quantify embedded anomalies and characterize variable soil/rock layers, as the propagation properties of seismic waves are modulated by the anomalies and layer interfaces. Both V_S and V_P structures could be inverted independently to increase the credibility of characterized profiles.

Many algorithms for waveform inversion have been developed and applied to synthetic and real seismic data in 2-D and 3-D large-scale (kilometers scale) domains. Due to computational challenges, the 3-D FWI algorithms often use acoustic modelling, therefore neglecting elastic effects. The acoustic approximation generally performs well for marine hydrophone data but is limited for land seismic data due to the importance of shear waves (Butzer et al. 2013), and thus cannot be used for geotechnical site investigation. Studies on elastic 3-D FWI are rare.

This paper presents a new 3-D FWI method for geotechnical site characterization. The method is based on a solution of 3-D elastic wave equations for forward modeling to simulate wave propagation, and a cross-adjoint gradient approach for model updating to extract material property. The seismic wavefields are acquired from geophysical testing using receivers and sources located in uniform 2-D grids on the ground surface, and then inverted for the extraction of 3-D subsurface wave velocity structures. For demonstration, the method was tested on synthetic datasets generated from realistic subsurface profiles with variable high- and low-velocity soil layers. It was also applied to field experimental dataset collected at a Florida test site, and FWI results are compared with invasive SPT N-values for verification.

FULL WAVEFORM INVERSION METHODOLOGY

The presented 3-D FWI method includes forward modeling to generate synthetic wave fields, as well as use of the adjoint gradient method to update model parameters (soil/rock wave velocities). For the forward modeling, the classic velocity-stress staggered-grid finite difference method in the time domain (Virieux, 1986) was used in combination with perfectly matched layer boundary conditions (Komatitsch and Martin, 2007) to solve the equations. For model updating, the gradient approach is used to minimize the residual between the estimated responses obtained by forward simulation and the observed seismic data.

Forward modeling of 3-D wave propagation

Three-dimensional elastic wave propagation is modelled by a set of the first-order linear partial differential equations for isotropic materials. The first set of three equations governs particle velocities, while the second set of six equations governs the stress-strain tensors.

$$\begin{cases} \dot{v}_x = \frac{1}{\rho}\left(\frac{\partial \sigma_{xx}}{\partial x} + \frac{\partial \sigma_{xy}}{\partial y} + \frac{\partial \sigma_{xz}}{\partial z}\right) \\ \dot{v}_y = \frac{1}{\rho}\left(\frac{\partial \sigma_{xy}}{\partial x} + \frac{\partial \sigma_{yy}}{\partial y} + \frac{\partial \sigma_{yz}}{\partial z}\right) \\ \dot{v}_z = \frac{1}{\rho}\left(\frac{\partial \sigma_{xz}}{\partial x} + \frac{\partial \sigma_{yz}}{\partial y} + \frac{\partial \sigma_{zz}}{\partial z}\right) \end{cases}$$

$$\begin{cases} \dot{\sigma}_{xx} = (\lambda + 2\mu)\frac{\partial v_x}{\partial x} + \lambda\left(\frac{\partial v_y}{\partial y} + \frac{\partial v_z}{\partial z}\right) \\ \dot{\sigma}_{yy} = (\lambda + 2\mu)\frac{\partial v_y}{\partial y} + \lambda\left(\frac{\partial v_x}{\partial x} + \frac{\partial v_z}{\partial z}\right) \\ \dot{\sigma}_{zz} = (\lambda + 2\mu)\frac{\partial v_z}{\partial z} + \lambda\left(\frac{\partial v_x}{\partial x} + \frac{\partial v_y}{\partial y}\right) \\ \dot{\sigma}_{xy} = \mu\left(\frac{\partial v_x}{\partial y} + \frac{\partial v_y}{\partial x}\right) \\ \dot{\sigma}_{xz} = \mu\left(\frac{\partial v_x}{\partial z} + \frac{\partial v_z}{\partial x}\right) \\ \dot{\sigma}_{yz} = \mu\left(\frac{\partial v_y}{\partial z} + \frac{\partial v_z}{\partial y}\right) \end{cases}$$

Where (v_x, v_y, v_z) is the particle velocity vector, $(\sigma_{xx}, \sigma_{yy}, \sigma_{zz}, \sigma_{xy}, \sigma_{xz}, \sigma_{yz})$ is the stress tensor, ρ is the mass density and μ, λ are Lamé's coefficients, the over-dot denotes a time derivative.

An accurate free-surface boundary condition is implemented by using the explicit finite difference and image technique (Robertsson, 1996), while the perfectly matched layers (PML) are applied at the other boundaries. The PML is an added zone surrounding the domain of interest to absorb energy of outgoing waves, and it is an efficient method for domain truncation (Fathi et al., 2015). As an example, Fig. 1 presents 3-D wave propagation in a homogeneous medium with and without the PML conditions. The medium has V_S of 200 m/s and V_P of 400 m/s for the entire domain. The source is located on the free surface (depth z =0). With the implementation of the PML, almost no reflected signals from boundaries are observed (Fig.1, left column). Whereas, significant reflected signals from boundaries are seen after 0.3 s (Fig.1, right column) without the PML.

Model updating by the cross-adjoint gradient method

For model updating, the classic cross-adjoint gradient method (Tarantola, 1984; Mora, 1987) is used to minimize the residual between the estimated data from the forward simulation and the observed (measured) waveform data, or a least-squares error $E(\boldsymbol{m})$:

$E(\boldsymbol{m}) = \frac{1}{2}\Delta\boldsymbol{u}^t\Delta\boldsymbol{u}$, where $\Delta\boldsymbol{u} = \{\Delta u_{i,j}, i = 1,..,NS,\ \ j = 1,..,NR\}$

$\Delta u_{i,j}(t) = \int_0^t F_{i,j}(\boldsymbol{m},\tau)d\tau - \int_0^t d_{i,j}(\tau)d\tau$; $d_{i,j}$ and $F_{i,j}(\boldsymbol{m})$ are the time-domain observed data (vertical particle velocity) and estimated data associated with the model $\boldsymbol{m}$ (V_S and V_P of cells) from the forward simulation for shot i and receiver j. $\Delta\boldsymbol{u}$ is the displacement residual vector, which is a combination of residuals from all receivers and shots. NS and NR are the numbers of shots and receivers.

The gradients of the least-squares error E with respect to λ and μ can be calculated using the adjoint-state method in the time domain (Plessiz, 2006; Butzer et al., 2013):

$$\delta\lambda = -\sum_{i=1}^{NS}\int_0^T dt\left[\left(\frac{\partial u_x}{\partial x} + \frac{\partial u_y}{\partial y}\right)\left(\frac{\partial \psi_x}{\partial x} + \frac{\partial \psi_y}{\partial y}\right) + \left(\frac{\partial u_x}{\partial x} + \frac{\partial u_z}{\partial z}\right)\left(\frac{\partial \psi_x}{\partial x} + \frac{\partial \psi_z}{\partial z}\right) + \left(\frac{\partial u_y}{\partial y} + \frac{\partial u_z}{\partial z}\right)\left(\frac{\partial \psi_y}{\partial y} + \frac{\partial \psi_z}{\partial z}\right)\right]$$

$$\delta\mu = -\sum_{i=1}^{NS}\int_{0}^{T} dt\left[\left(\frac{\partial u_x}{\partial y}+\frac{\partial u_y}{\partial x}\right)\left(\frac{\partial \psi_x}{\partial y}+\frac{\partial \psi_y}{\partial x}\right)+\left(\frac{\partial u_x}{\partial z}+\frac{\partial u_z}{\partial x}\right)\left(\frac{\partial \psi_x}{\partial z}+\frac{\partial \psi_z}{\partial x}\right)+\left(\frac{\partial u_y}{\partial z}+\frac{\partial u_z}{\partial y}\right)\left(\frac{\partial \psi_y}{\partial z}+\frac{\partial \psi_x}{\partial z}\right)\right.$$
$$\left.+2\left(\frac{\partial u_x}{\partial x}\frac{\partial \psi_x}{\partial x}+\frac{\partial u_y}{\partial y}\frac{\partial \psi_y}{\partial y}+\frac{\partial u_z}{\partial z}\frac{\partial \psi_z}{\partial z}\right)\right]$$

Where u_k and ψ_k are the forward and backward wavefields, with k denoting spatial direction x, y, or z. Based on the wave velocity and Lame's coefficient relationships, the gradients of the least-squares error E with respect to V_S and V_P are calculated as:

$$\delta V_P = 2\rho V_P \delta\lambda$$
$$\delta V_S = -4\rho V_S \delta\lambda + 2\rho V_S \delta\mu$$

Finally, V_S and V_P of cells at iteration n+1 is updated from iteration n as:

$$V_P{}^{n+1} = V_P{}^{n} - \alpha_P \delta V_P$$
$$V_S{}^{n+1} = V_S{}^{n} - \alpha_S \delta V_S$$

Where α_P, α_S are optimal step lengths, which are estimated by parabola fitting (Rosenbrock, 1960). During the inversion, the mass density is kept constant for the whole domain. The V_S and V_P of cells are updated iteratively. The inversion analysis is stopped when no optimal step length is found (no better model) or the maximum number of iterations is reached.

Application on synthetic data

Synthetic studies allow data from specific scenarios to be generated for inversion. Synthetic model refers to an earth model, whose velocity profile (V_S and V_P of cells) is assumed or known a priori. Using a known velocity structure, surface waveform data is calculated for an assumed test configuration (i.e. 2-D uniform grids of shots and receivers). The waveform data are then input to the inversion program as if they were acquired from a field test. Inverting the data produces 3-D profiles of V_S and V_P structures, which lies directly below the receiver and shot area. Theoretically, the interpreted velocity profile should be the same as the model assumed at the start.

The synthetic model is 18 m deep, 36 m long and 9 m wide, consisting of 3 soil layers (Fig. 3a) with a low-velocity second layer. The 3 layers have V_S of 400 m/s, 200 m/s and 600 m/s, and V_P of 800 m/s, 400 m/s and 1200 m/s (twice that of V_S). For synthetic data generation, the test configuration (Fig. 2) includes 96 receivers and 52 shots (sources) located in 2-D uniform grids. The receiver grid is 4 × 24 at 3 m and 1.5 m spacing in shorter and longer directions respectively, and the source grid is 4 x 13 at 3 m spacing in both directions. The waveform data were created up to 30 Hz using forward simulation (solutions of Eqs. 1 and 2) for 52 shots, and recorded at the 96 receiver locations. Both shots and receivers were on the free surface (0-m depth). The Ricker wavelet was used for the source signature, and the recorded time was 0.9 s.

Two inversion runs were conducted for data at frequency bandwidths: 5 - 20 Hz and 5 - 30 Hz. The analysis began with a 1-D initial model with linearly increasing velocities with depth (Fig. 3b). The initial V_S profile increases from 400 m/s on the free surface (0-m depth) to 600 m/s at the bottom of the model (18-m depth), and the V_P is twice that of the V_S. It is noted that no prior information of the low-velocity layer is included in the initial model. The gradients and the optimal step length were calculated to update model at each iteration. The inversion process stopped after 20 iterations for each run. The complete analysis took about 17 hours on a work station computer (32 cores of 3.46 GHz each and 256 GB of memory).

The final inverted result is shown in Fig. 3c, which is similar to the true model (Fig. 3a). The layer interfaces were accurately characterized. True V_S and V_P values of the 3 layers were

recovered, including the low-velocity second layer. The 3-D FWI algorithm has great potential for characterization of challenging site conditions with variable high- and low-velocity layers.

Application on real data

Obtaining great results on synthetic waveform dataset, the presented 3-D FWI method was then applied to field experimental data. The test site was a dry retention pond in Gainesville, Florida (Fig. 4a). The same test configuration of 96 receivers and 52 shots (Fig. 2) was used for the field seismic survey. The receiver grid was 4 × 24 and the source grid was 4 × 13. The seismic wavefields were generated by a propelled energy generator (PEG, 40 kg model) as shown in Fig. 4b, and simultaneously recorded by 48 4.5-Hz vertical geophones in two stages. In stage one, the 48 geophones were placed at the first half of the receiver grid (the first 2 lines, 24 geophones each line), and 52 shots were conducted for the entire source grid. In stage two, the 48 geophones were placed at the second half of the receiver grid (the last 2 lines, 24 geophones each line), and 52 shots were repeated. As the PEG generated the same impact load (constant drop weight and height) at every shot location, the collected data from the two stages were simply combined to produce 96-channel shot gathers. Four standard penetration tests (SPT) were also conducted at distance 24 m on each geophone lines for verification of seismic results.

For inversion analysis, appropriate initial models are required to avoid cycle skipping that produces inaccurate local solutions. From the synthetic study, 1-D initial models of increasing wave velocities with depth were sufficient to invert the variable profile with high- and low-velocity layers. Via spectral analysis of measured data, Rayleigh wave velocities were determined from 250 to 400 m/s at the frequency range 12 to 50 Hz. As V_S is similar to Rayleigh wave velocity, the initial model was established having V_S increasing with depth from 250 m/s at the surface to 400 m/s at the bottom of the model (Fig. 5a). V_P was calculated from V_S and assumed Poisson's ratio of 0.33 for the entire medium. The depth of the model was simply assumed to be a half of the longer dimension of the test configuration as 18 m.

To further avoid local solutions, the inversion analysis was done in a sequence of increasing frequencies, as lower frequency data (large wavelengths) requires less details in initial models. Two inversion runs were conducted for filtered data sets at two frequency bandwidths: 5 - 20 Hz and 5 - 30 Hz with central frequencies of about 12 and 22 Hz, respectively. The first run at 5 - 20 Hz began with the initial model shown in Fig. 5a, and the second run began with the inverted result of the first run.

The 18 × 36 × 9 m (depth × length × width) medium was divided into cells of 0.75 × 0.75 × 0.75 m. The cell size of 0.75 m was selected as a half of the smaller geophone spacing (1.5 m), and used for both inversion runs. The optimal step length was determined for each iteration to update the model. V_S and V_P of cells were updated independently during inversion. Similar to the synthetic study, both inversion runs stopped at 20 iterations. The complete analysis took about 20 hours on the same computer used for the synthetic data analysis. Fig. 6 shows the observed and estimated waveforms at the 96 receivers for a sample shot located at x = 18 m, y = 6 m for the final iteration (iteration 40). The observed and estimated data are very similar, and no cycle skiping is observed; suggesting the 1-D initial model was sufficent.

The final inverted model for data at 5 - 30 Hz is shown in Fig. 5b. The V_S profile (Fig. 5b, top) consists of softer soil layers (V_S ~ 100 – 300 m/s) with an embedded low-velocity zone at shallow depths, underlain by a stiffer soil layer (V_S ~ 400 – 500 m/s). The V_P profile (Fig. 5b, bottom) is consistent with the V_S profile. For verification, Fig.7 presents the comparison between the inverted V_S and SPT 'N' values at 4 invasive test locations (Fig. 2). The seismic and SPT

results are generally consistent. Both show softer materials from 0 to 5-m depth, linearly increasing stiffness with depth from 5 to 10-m depth, and stiffer materials below 10-m depth. Interestingly, the low-velocity zone at about 5-m depth identified by the 3-D FWI analysis is confirmed by the SPT results.

CONCLUSION

A 3-D FWI method is presented for geotechnical site characterization. The method is based on a solution of 3-D elastic wave equations for forward modeling to simulate wave propagation, and a cross-adjoint gradient approach for model updating to extract material property. Seismic wave fields are acquired from geophysical testing using receivers and sources located in uniform 2-D grids on the ground surface, and then inverted for the extraction of 3-D subsurface wave velocity structures. The method was applied to both synthetic and field datasets. The results from a synthetic dataset suggest that the waveform analysis can characterize the subsurface profile with variable high- and low velocity layers. For the field data, both V_S and V_P of 3-D variable soil layers are characterized. There also appears to be good consistency between the V_S and SPT N-values, including identification of a buried low-velocity zone at 5-m depth. In addition, the 3-D FWI method is computationally practical; the presented results were all obtained within 20 hours on a standard desktop computer.

ACKNOWLEDGMENTS

This study was financially supported by the National Science Foundation, grant CMMI-1637557. The authors would like to thank the Florida Department of Transportation (FDOT) and the State Materials Office in Gainesville, Florida, for providing access to the test site and conducting SPT tests.

REFERENCES

Butzer S., Kurzmann A. and Bohlen T. (2013), "3D elastic full-waveform inversion of small-scale heterogeneities in transmission geometry", *Geophysical Prospecting,* 2013, 61, 1238–1251.

Fathi A., Kallivokas L., Poursartip B. (2015) Full waveform inversion in three-dimensional PML-truncated elastic media: *Comput Methods Appl Mech Eng.* arXiv:1408.6221

Kamatitsch D. and Martin R. (2007). An unsplit convolutional perfectly matched layer improved at grazing incidence for the seismic wave equation: *Geophysics;* 72(5), SM155–SM167.

P. Mora. Nonlinear twodimensional elastic inversion of multioffset seismic data. *Geophysics*, 52(9):1211–1228, 1987.

Plessix R.E. 2006. A review of the adjoint-state method for computing the gradient of a functional with geophysical applications. *Geophysical Journal International* 167, 495–503.

Robertsson, J. O. A., (1996). A numerical free-surface condition for elastic/viscoelastic finite-difference modeling in the presence of topography, *Geophysics*, 61, 1921–1934.

Rosenbrock H. An automatic method for finding the greatest or least value o f a function. *The Computer Journal*, 3:175–184, 1960.

Virieux J. (1986). P–SV wave propagation in heterogeneous media: velocity–stress finite-difference method: *Geophysics*; 51(4): 889–901

Tarantola, A., 1984, Inversion of seismic reflection data in the acoustic approximation: Geophysics, 49, 1259–1266, doi: 10.1190/1.1441754.

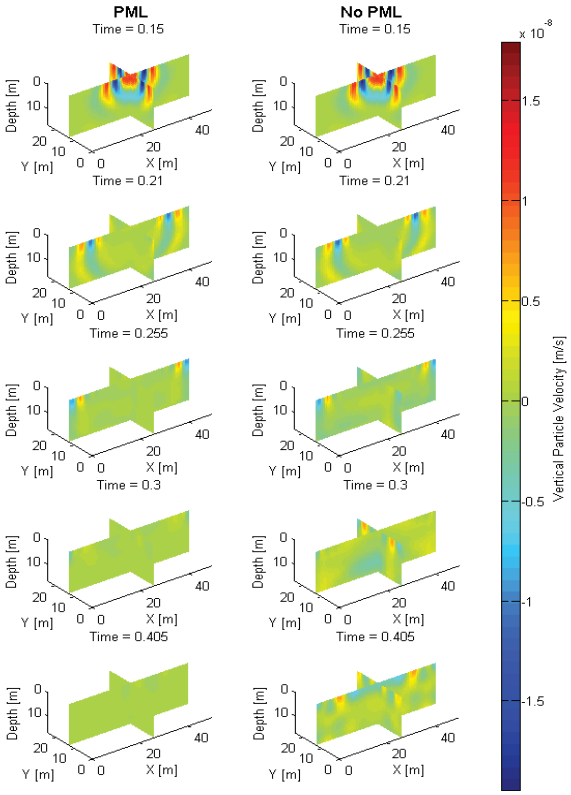

Figure 1. 3-D wave propagation with and without the PML

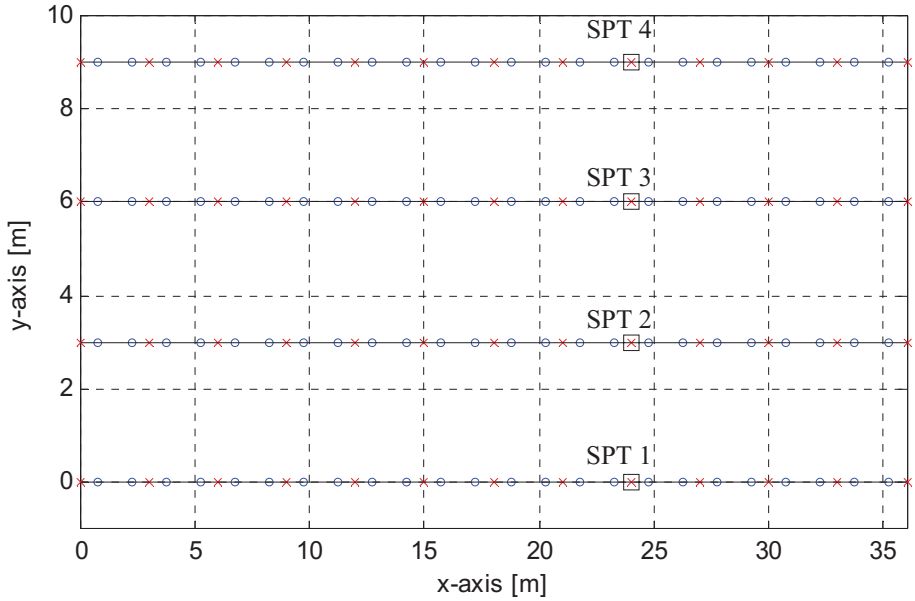

Figure 2. Test configuration used for both synthetic and field experiments: source (cross), receiver (circle). Standard penetration tests, SPT (square) are only for the field experiment.

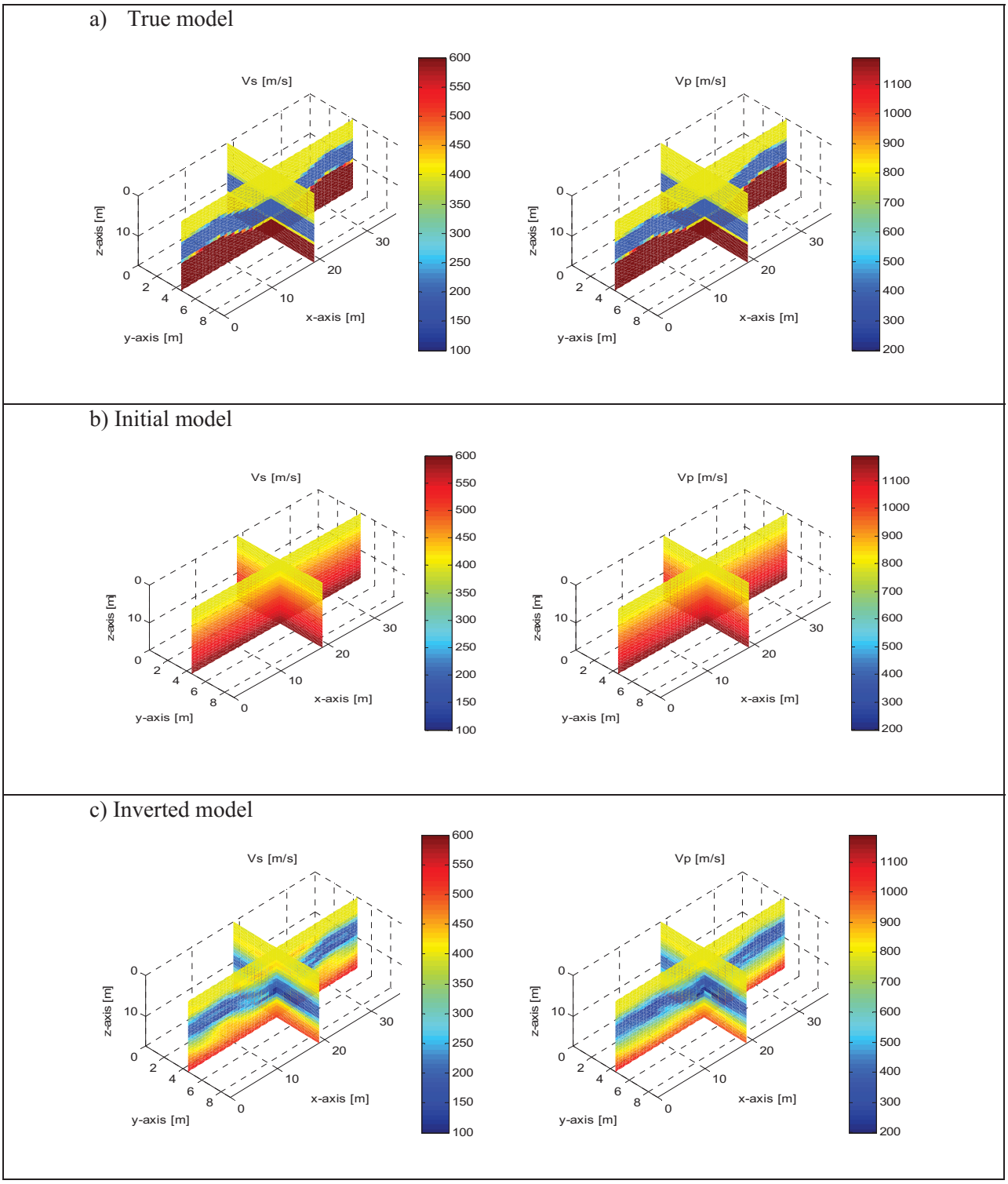

Figure 3. Synthetic model: distribution of V_S and V_P (m/s): a) true model used to generate synthetic data for inversion analysis; b) initial model used at the beginning of inversion; and c) final inverted models respectively.

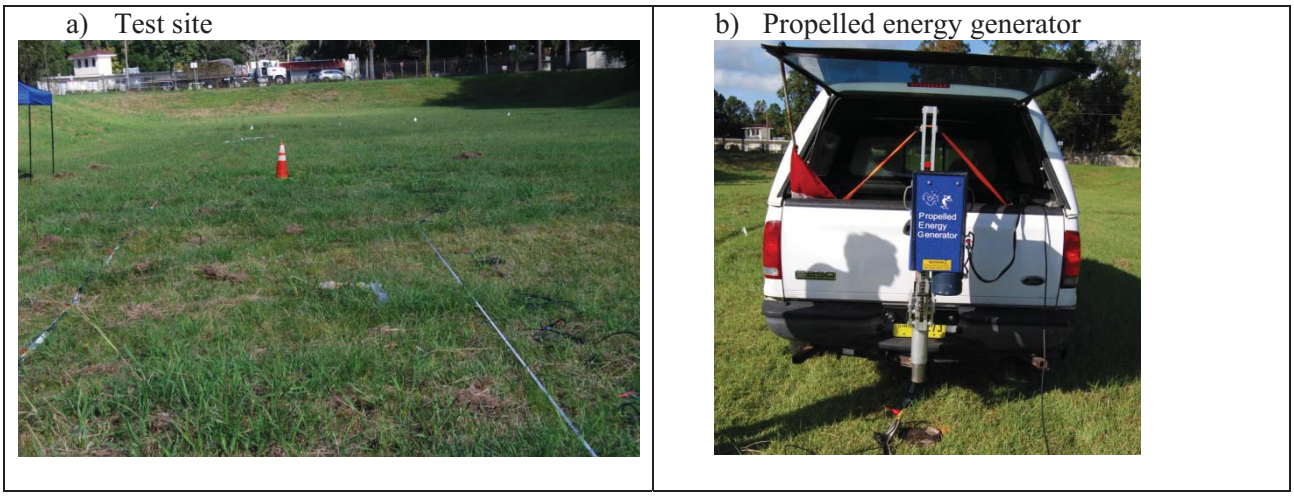

Figure 4. Field experiment: test site and propelled energy generator

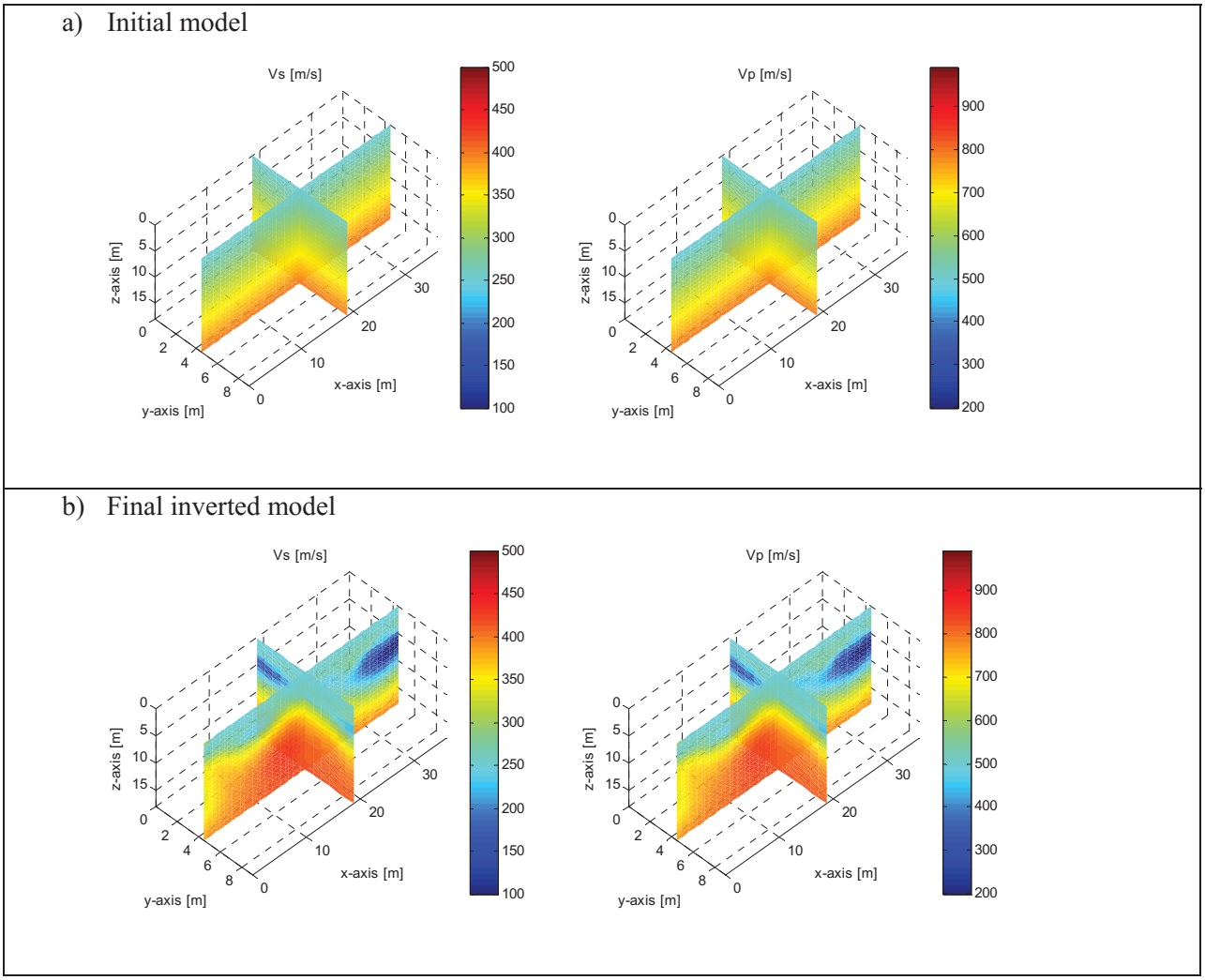

Figure 5. Field experiment: distribution of V_S and V_P (m/s): a) initial model used at the beginning of inversion; and b) final inverted model at 5-30 Hz.

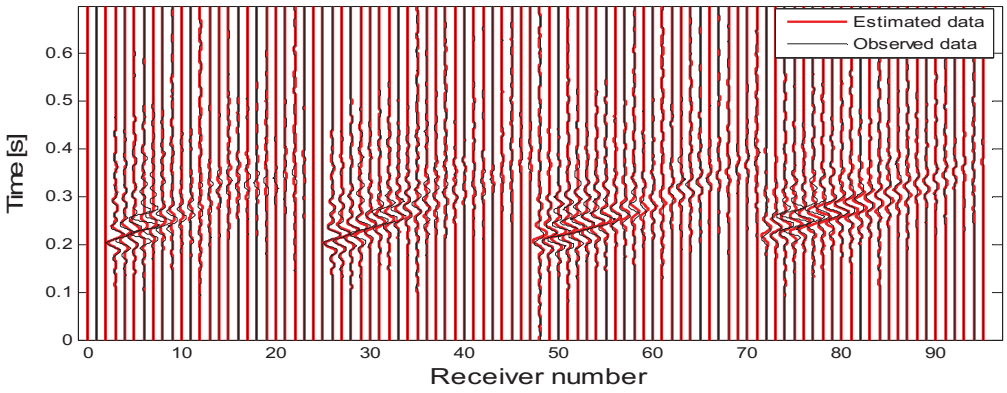

Figure 6. Field experiment: waveform comparison for a sample shot at last iteration.

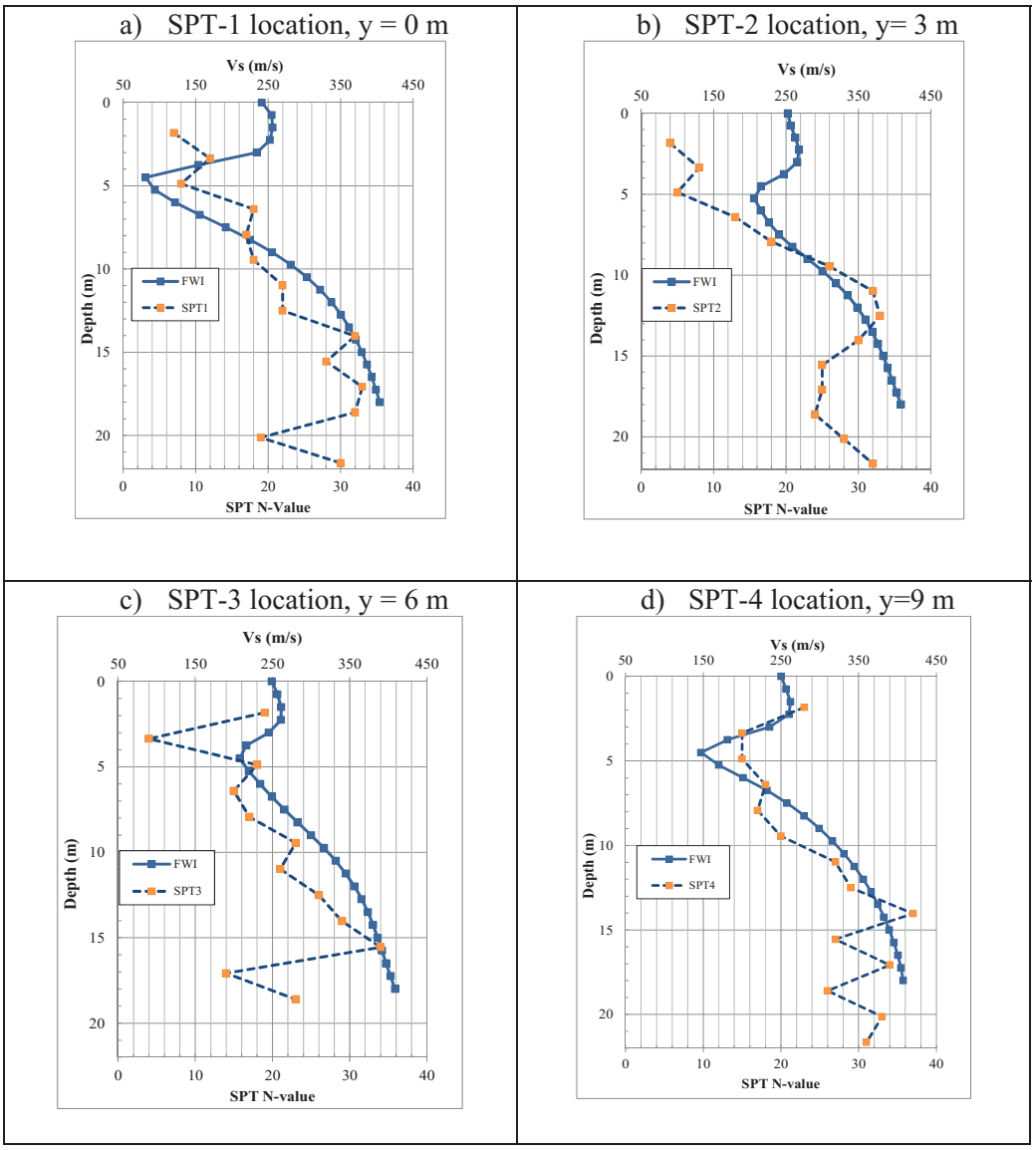

Figure 7. Comparison between Vs and SPT 'N' values at the 4 invasive test locations